

Formation of the Donor–Acceptor Charge-Transfer Exciton and Its Contribution to Charge Photogeneration and Recombination in Small-Molecule Bulk Heterojunctions

M. J. Kendrick,[†] A. Neunzert,[†] M. M. Payne,[‡] B. Purushothaman,[‡] B. D. Rose,[§] J. E. Anthony,[‡] M. M. Haley,[§] and O. Ostroverkhova^{*,†}

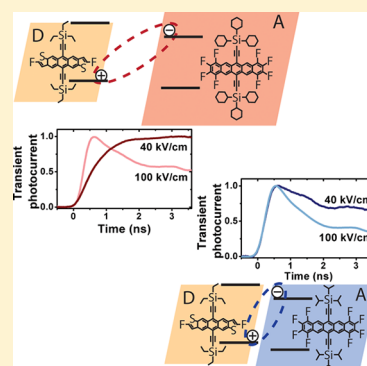
[†]Department of Physics, Oregon State University, Corvallis, Oregon 97331, United States

[‡]Department of Chemistry, University of Kentucky, Lexington, Kentucky 40506, United States

[§]Department of Chemistry, University of Oregon, Eugene, Oregon 97403, United States

Supporting Information

ABSTRACT: We report on the formation of charge-transfer (CT) excitons and their effect on photocurrent dynamics in composites with a fluorinated anthradithiophene (ADT-TES-F) donor (D) and acceptors (A) with (i) various LUMO energy offsets with respect to that of the donor (Δ LUMO) and (ii) several different side groups that modify spatial D/A separation at the D/A interface. Exciplexes and nonemissive CT excitons were formed in composites with Δ LUMO <0.6 and >0.6 eV, respectively. A competition between fast charge carrier photogeneration and CT exciton formation was observed, with outcomes depending on the applied electric field (E) and on the D/A separation. At low E fields, CT formation was dominant, and up to a factor of 2 increase in charge photogeneration efficiency due to CT exciton dissociation was observed in composites with large spatial D/A separation compared with that in pristine D films. At high E fields, fast charge carrier photogeneration was dominant in all composites, and no improvement in charge photogeneration efficiency with respect to that in pristine D films was observed. Dramatic changes in charge recombination dynamics were observed depending on the spatial D/A separation. These contributed to a factor of 5–10 improvement in continuous-wave photocurrents in composites with large spatial D/A separation as compared with those in pristine D films.



1. INTRODUCTION

Organic optoelectronic materials have drawn interest based on their low cost and tunable properties and have shown promise in a wide range of applications, from display technologies to photovoltaics.^{1,2} Additionally, solution-processable organics can be combined into composite materials, which can have drastically different optical and electronic properties and can be tailored for specific applications. For example, organic bulk heterojunctions (BHJs) have been utilized in solar cells,³ photodetectors,⁴ and photorefractive devices⁵ due to enhanced photogeneration of charge carriers that results from photo-induced electron transfer between donor (D) and (A) acceptor molecules with properly offset HOMO and LUMO energies.⁶ Currently, most high-performance BHJs are combinations of a photoconductive polymer donor with fullerene-based acceptors; however, the performance of small-molecule BHJs^{7–10} is rapidly improving, with several small-molecule-based materials exhibiting power conversion efficiencies (PCEs) of 6 to 7%.^{11,12}

The relative HOMO and LUMO energies of the D and A and molecular packing at the D/A interface have been identified as key factors in efficient charge photogeneration.^{6,13–19} However, the mechanisms driving the evolution of an exciton created by an absorbed photon in the donor to free charge carriers, especially those involving the formation of

intermediate bound charge-transfer (CT) states shared between adjacent D and A molecules, and how they depend on the D and A HOMO and LUMO energies and molecular alignment at the D/A interface are still under investigation.^{6,17,20–24} In particular, the relationship between properties of CT excitons and photocurrent is not well understood^{6,17,25,26} and is important to address for the development of efficient BHJs. Most work aiming to quantify properties of CT states and their effect on the photoconductive performance of BHJs has been done in polymer-based D/A systems,^{27–31} primarily polymer/fullerene blends,³² whereas considerably less is known about similar issues in small-molecule BHJs.^{33–35} In this article, we explore the effects of (i) the offset in HOMO and LUMO energies of D and A and (ii) the molecular packing at the D/A interface on CT state formation, exciton dynamics, and photocurrent in small-molecule BHJs. We show that the spatial D/A separation at the D/A interface plays a crucial role in the properties of CT states and their contribution to the photocurrent and that it dominates over effects of the D/A LUMO energy offsets.

Received: June 15, 2012

Revised: July 30, 2012

Published: August 10, 2012

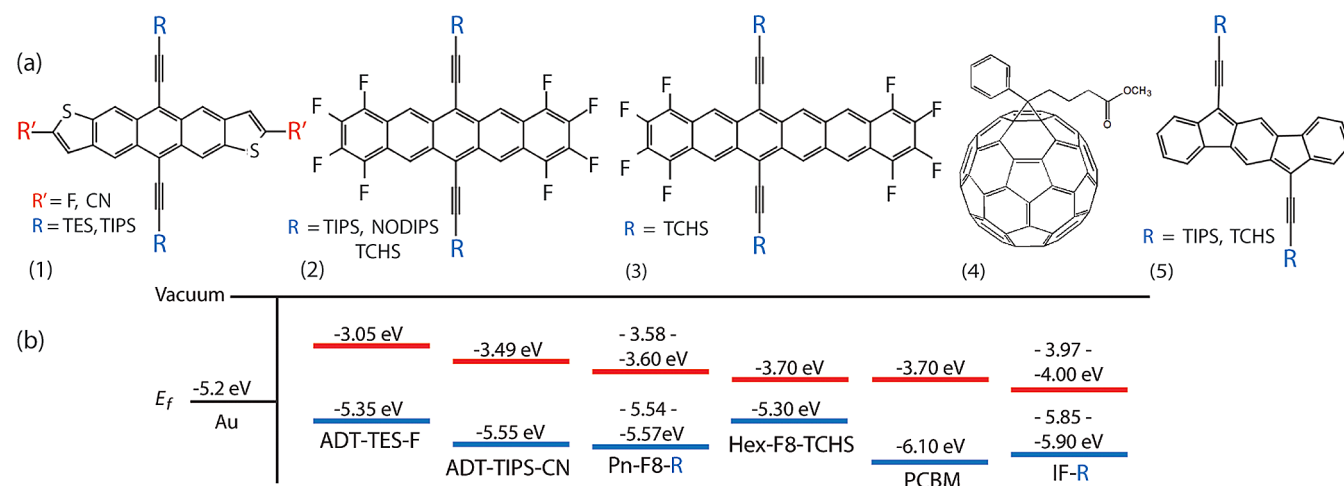


Figure 1. (a) Molecular structures of the donor (a.1, ADT-TES-F: R = TES, R' = F) and acceptors used in our studies: (a.1) ADT-TIPS-CN: R = TIPS, R' = CN; (a.2) Pn derivatives; (a.3) Hex derivative; (a.4) PCBM; and (a.5) IF derivatives. (b) HOMO and LUMO energies of molecules under study.

Table 1. Electrochemical, Optical, and Photoluminescent Properties of Molecules

molecule	HOMO–LUMO gap	E_{gap} , eV ^a	λ_{abs} , nm ^b	λ_{PL} , nm ^b	$E_{\text{opt.gap}}$, eV ^c	E_{DA} , eV ^d	ΔG_{CT} , eV ^e	ΔG_{ET} , eV ^f	$\Delta G_{\text{CT}} - \Delta G_{\text{ET}}$, eV
ADT-TES-F	2.3		528	536	2.31				
ADT-TIPS-CN	2.06		582	590	2.1	1.86	-0.45	-0.21	-0.24
Pn-F8-NODIPS	1.96		635	645	1.92	1.76	-0.55	-0.39	-0.16
Hex-F8-TCHS	1.6		739	800	1.55	1.65	-0.66	-0.76	0.1
IF-TIPS	1.9		572		1.77 ^g	1.35	-0.96	-0.54	-0.42

^aObtained from DPV or CV measurements. ^bWavelength of lowest energy absorption maximum or of maximal PL in dilute toluene solutions. ^cEnergy corresponding to maximal PL emission of molecules in solution or dispersed in a host matrix at low concentrations.³⁹ ^dDifference between the LUMO energy of the A and HOMO energy of the D. ^e $\Delta G_{\text{CT}} = E_{\text{DA}} - E_{\text{opt.gap}}(\text{D})$. ^f $\Delta G_{\text{ET}} = E_{\text{opt.gap}}(\text{A}) - E_{\text{opt.gap}}(\text{D})$. ^gIF-TIPS exhibited no measurable PL emission; the optical gap was estimated from the time-dependent density functional theory (TD-B3LYP/6-311+G(d,p)//B3LYP/6-31G(d)).

Table 2. Electrochemical, Crystallographic, Photoluminescent, and Photoconductive Properties of Films

material	ΔLUMO , eV	volume of R (volume/molecule), Å ^{3a}	$E_{\text{CT}}(E_{\text{DA}})$, eV ^b	$I_{\text{PL}}(\text{D/A})/I_{\text{PL}}(\text{D/ADT-TIPS-CN})$ exciplex ^c	$t_{\text{ph,max}}$ (ns) at 20 (100), kV/cm ^d
pristine ADT-TES-F		204 (807)			<0.6 (<0.6)
D/A composites					
ADT-TIPS-CN	0.44	278.5 (1051)	1.86 (1.86)	1	<0.6 (<0.6)
Pn-F8-NODIPS	0.53	402.5 (1246)	1.72 (1.76)	0.064 ± 0.004	3.3 (<0.6)
Pn-F8-TCHS	0.54	469.2	1.75 (1.77)	0.021 ± 0.001	2.4 (<0.6)
Pn-F8-TIPS	0.55	278.5 (988)	1.72 (1.75)	0.21 ± 0.03	<0.6 (<0.6)
Hex-F8-TCHS	0.65	469.2 (1580)	(1.65)		2.2 (<0.6)
PCBM	0.65	(1053–1948) ^e	(1.65)		2.8 (<0.6)
IF-TCHS	0.92	469.2 (1209)	(1.38)		3.3 (<0.6)
IF-TIPS	0.95	278.5 (928)	(1.35)		<0.6 (<0.6)

^aVolume of a side group R calculated from crystallographic data. The number in parentheses is a unit cell volume (from CIF files) divided by the number of molecules in the unit cell. ^bEnergy of the CT state obtained from peak PL emission from the exciplex. The value in parentheses is the difference between the LUMO energy of the A and HOMO energy of the D. ^cExciplex PL obtained from integrated exciplex PL spectra in various D/A composites with respect to that in the composite with ADT-TIPS-CN acceptor. Error reflects sample-to-sample variation. ^dTime at which the transient photocurrent reached maximum at the applied E field of 20 kV/cm (100 kV/cm). ^eValues depend on the solvent used for sample preparation and were taken from ref S1.

2. EXPERIMENTAL PART

2.1. Materials. In all D/A composites, a high-performance ADT-TES-F derivative (Figure 1a.1) was used as the donor. This ADT derivative exhibited high charge carrier (hole) mobilities (>1.5 cm²/(Vs) in thin-film transistors),^{36,37} high photoconductive gains, and relatively strong photoluminescence (PL) in solution-deposited polycrystalline films.^{38,39} To explore effects of D and A HOMO and LUMO energy offsets,

we chose multiple acceptors with various HOMO and LUMO energies that, for example, yielded LUMO offsets (ΔLUMO) ranging between 0.44 and 0.95 eV (Figure 1b and Tables 1 and 2). This range is of interest, as numerical modeling predicted the highest PCEs at a ΔLUMO of ~0.55 eV and fill factor saturation at ~1 eV.⁶ To explore D/A molecular packing effects, different groups of acceptor molecules were chosen, such as pentacene (Pn) and indenofluorene (IF) derivatives,

which have similar HOMO and LUMO energies but are functionalized with side groups (R in Figure 1a) of different sizes that yield different packing motifs in the solid state.^{40,41} In particular, the following acceptor molecules were employed: (i) ADT-TIPS-CN, Figure 1a.1;^{34,35} (ii) three fluorinated Pn derivatives with TIPS,⁴² NODIPS, and TCHS side groups (Pn-F8-R, Figure 1a.2); (iii) a fluorinated hexacene (Hex) derivative with TCHS side groups (Hex-F8-TCHS, Figure 1a.3);⁴³ (iv) two IF derivatives with TIPS and TCHS side groups (IF-R, Figure 1a.5);^{44,45} and (v) PCBM (Figure 1a.4, from Sigma-Aldrich). HOMO and LUMO energies for molecules under study, measured in solution using differential pulse voltammetry (DPV)³⁸ or cyclic voltammetry (CV),⁴⁴ are shown in Figure 1b. The values for PCBM, which vary considerably in the literature, were taken from the Sigma-Aldrich data sheet and are also consistent with those previously measured by DPV.³² Molecular structures for side groups are shown in Figure 2.

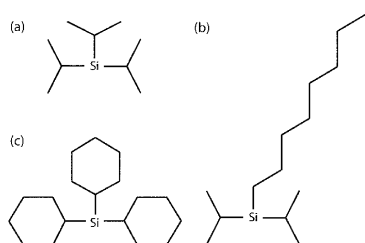


Figure 2. Chemical structure of the side groups R. (a) TIPS, (b) NODIPS, and (c) TCHS.

Optical absorption and PL spectra for molecules in solution are provided in Figure S1 of the Supporting Information (SI) and are summarized in Table 1. Although the exact D and A molecular arrangement at the D/A interface is not known, the approximate volume of the side group R and/or average volume per molecule calculated from crystallographic data for the D and A molecules (Table 2) provided a relative measure of separation between the D and A molecules in the solid state. For example, in composites with Pn acceptors, the largest D/A separation at the D/A interface would be expected with large TCHS substituent, followed by NODIPS and TIPS side groups.

2.2. Sample Preparation. In our study, 6 mM solutions of ADT-TES-F in toluene and 2 wt % acceptor/98 wt % donor mixtures in toluene were used to drop-cast pristine ADT-TES-F (pristine D) and composite films, respectively. For all drop-cast films, substrates were placed on a hot plate at ~ 65 °C, and multiple ~ 10 μ L drops were dispensed slowly using a pipettor to control film formation over the photolithographically deposited Cr/Au (5 nm/50 nm) interdigitated electrode pairs. Each interdigitated electrode pair consisted of 10 pairs of 1 mm long and 25 μ m wide fingers, with a 25 μ m gap between the fingers of opposing electrodes. This preparation method yielded polycrystalline films, as confirmed by X-ray diffraction (e.g., Figure S2 of the Supporting Information).^{36,37,46}

The low concentration of acceptor molecules was chosen to minimize the disruption of film crystallinity⁴⁷ and thus prevent reduction in hole mobility. Additionally, this enabled us to relate the photocurrent dynamics to properties of the CT states while neglecting effects of acceptor aggregation, acceptor domain formation, and electron mobility in the acceptor domains.¹³

2.3. Optical Absorption and PL Measurements. For optical absorption measurements in solution and film, light from a halogen lamp (LS-1, Ocean Optics) transmitted through samples was measured using an Ocean Optics USB2000 spectrometer. Measurements of optical absorption and PL emission in films were conducted on an inverted microscope (Olympus IX-71) with a 10 \times objective. For PL spectral measurements, films were excited in a wide-field geometry with 532 nm light (frequency-doubled Nd:YVO₄ laser from Coherent). PL emission was collected through a 560DCLP dichroic mirror (Omega Optical) to filter out scatter at the excitation wavelength into an Ocean Optics USB2000 spectrometer calibrated to a 3100 K halogen lamp.

PL lifetime measurements were taken under 400 nm excitation from a frequency-doubled 80 fs Ti:sapphire laser. A time-correlated single-photon counter (TCSPC) board (PicoQuant TimeHarp 200) was used with a single-photon avalanche photodiode (SPAD – Molecular Photonic Devices) for detection.³⁸ Combinations of a 420DCLP dichroic mirror (Omega Optical), a 3RD440LP long pass filter (Omega Optical), and a D740/80 \times band-pass filter (Chroma Tech.) were used to measure the lifetimes of either ADT-TES-F or exciplex PL. The instrument response function (IRF) (~ 200 ps) was recorded using scattered light from a frosted microscope slide. The PL lifetime decays (I_{PL}) were fit with a single-exponential function ($I_{PL} \approx C \exp[-t/\tau]$) to determine the amplitude C and the lifetime τ .

For electric-field-dependent measurements of optical absorption, PL spectra, and PL lifetimes, voltage was applied to the samples using a Keithley 237 source-measure unit. The measurements described above were performed as a function of applied voltage (V) ranging from 0 to 250 V. The average applied electric field (E) was calculated using $E = V/L$, where L is the gap between the electrodes.

2.4. Transient and Continuous-Wave Photocurrent Measurements. For transient photocurrent measurements, a 355 nm, 0.18 μ J/cm², ~ 500 ps pulsed excitation (cavity Q-switched frequency-tripled Nd:YAG laser, 44.6 kHz, from Nanolase) source was used to illuminate samples from the substrate side. Voltage was applied to samples mounted in custom-made fixtures using a Keithley 237 source-measure unit. Transient photocurrents were measured using either a 50 GHz digital sampling oscilloscope (DSO) (CSA8200/Tek80E01) with a Centellax UAOL65VM broadband amplifier (100 kHz to 65 GHz) for measurements on nanosecond time scales or a 300 MHz DSO (Agilent DSO6032A) for measurements on microsecond time scales. The time resolution of the experimental setup was ~ 0.6 ns, limited by the laser pulse width and jitter. In pristine ADT-TES-F films under these photoexcitation conditions, the photocurrents reached ~ 175 μ A at 100 kV/cm.

Continuous-wave (cw) photocurrents in films were measured under 532 nm (frequency-doubled Nd:YVO₄ laser from Coherent) 3 mW/cm² or broad-band ~ 300 –400 nm, peaked at ~ 370 nm (96 000 solar simulator (Newport) with a dichroic mirror (Oriel 81045), a UV band-pass filter (Oriel 81046), and a color glass filter (BG39, CVI)), 2 mW/cm² photoexcitation. For both dark and photocurrent measurements, voltage was applied to the samples, and current was measured using a Keithley 237 source-measure unit. Photocurrent was calculated as the difference between the current measured under photoexcitation and the dark current. In pristine ADT-TES-F films under these photoexcitation conditions, the photocurrents

reached $\sim 40 \mu\text{A}$ ($12 \mu\text{A}$) at 532 nm ($\sim 370 \text{ nm}$) excitation at 40 kV/cm.

All measurements were conducted at room temperature.

3. RESULTS AND DISCUSSION

3.1. Charge versus Energy Transfer: Basic Considerations. To estimate whether charge or energy transfer would be the dominant interaction in D/A composites, we calculated the change in the free energy upon charge (ΔG_{CT}) and energy (ΔG_{ET}) transfer from D to A as follows:⁴⁸ $\Delta G_{\text{CT}} = E_{\text{DA}} - E_{\text{opt,gap}}(\text{D})$ and $\Delta G_{\text{ET}} = E_{\text{opt,gap}}(\text{A}) - E_{\text{opt,gap}}(\text{D})$. Here E_{DA} is the difference between LUMO energy of the A and HOMO energy of the D, and $E_{\text{opt,gap}}(\text{D or A})$ is the optical gap obtained from the maximal PL emission in the spectra of the ADT-TES-F donor or acceptors, respectively. Table 1 shows ΔG_{CT} and ΔG_{ET} values as well as their difference, $\Delta G_{\text{CT}} - \Delta G_{\text{ET}}$, calculated for several D/A composites. The negative values of the $\Delta G_{\text{CT}} - \Delta G_{\text{ET}}$ were observed for most composites under study. This, however, would not necessarily guarantee that charge transfer dominates over energy transfer in these composites. For example, in a variety of polymer composites, $\Delta G_{\text{CT}} - \Delta G_{\text{ET}}$ of below -0.35 eV was needed in order for the charge transfer to dominate.^{48,49} This additional energy of $\sim 0.35 \text{ eV}$ was attributed to the energy penalty occurring upon changing from an intra- to interchain exciton. If we apply similar considerations to the case of our small-molecule BHJs, then energy transfer would be expected to dominate in composites with ADT-TIPS-CN, Pn-F8-R, and Hex-F8-TCHS acceptors and charge transfer in composites with IF acceptors. Previous studies of ADT-TES-F/ADT-TIPS-CN composites identified strong energy transfer between the ADT-TES-F donor and the ADT-TIPS-CN acceptor in the presence of a spacer molecule (which is not expected to interact with either donor or acceptor molecules) such as PMMA. If no spacer molecule was used, however, then the dominant interaction was the formation of the CT emissive state (exciplex).³⁴ Interestingly, in our study, no evidence of energy transfer was observed in any of the composites under study; instead, in all composites, the CT state formation was favored, as discussed in the following sections. This could be due to a smaller energy change from intra- to intermolecular excitons in small-molecule BHJs so that any negative or even small positive difference $\Delta G_{\text{CT}} - \Delta G_{\text{ET}}$ would be sufficient for CT to dominate, especially in the case of a relatively poor overlap of the donor's PL and acceptor's absorption and large D/A separation (e.g., in the case of the Hex-F8-TCHS acceptor, Figure S1 of the Supporting Information).

With the above definition of the ΔG_{CT} , the absolute value of ΔG_{CT} is within 0.01 eV of the ΔLUMO (Tables 1 and 2). Because the exact definition of ΔG_{CT} could be ambiguous,^{27,48} in part due to aggregation effects on the optical absorption and PL spectra,³⁹ to avoid ambiguity in the following discussions, we will use ΔLUMO obtained from the DPV or CV measurements instead (Table 2).

3.2. Optical Absorption and PL Properties of D/A Composites. To explore changes in exciton dynamics depending on the acceptor, we measured the optical absorption and PL spectra and PL lifetime decays of films (Section 2.3). Absorption spectra of all composites were similar to those of the pristine D films (Figure S3 of the Supporting Information). Analysis of PL emission in pristine D films (Figure S4(a) of the Supporting Information), attributed to that of disordered H-aggregates, has been previously reported.^{35,38,39} In all

composites with A such that $\Delta\text{LUMO} < 0.6 \text{ eV}$ (i.e., Pn-F8-R and ADT-TIPS-CN), the formation of an emissive CT state (exciplex) was observed in PL data (Table 2 and Figure 3).^{34,35}

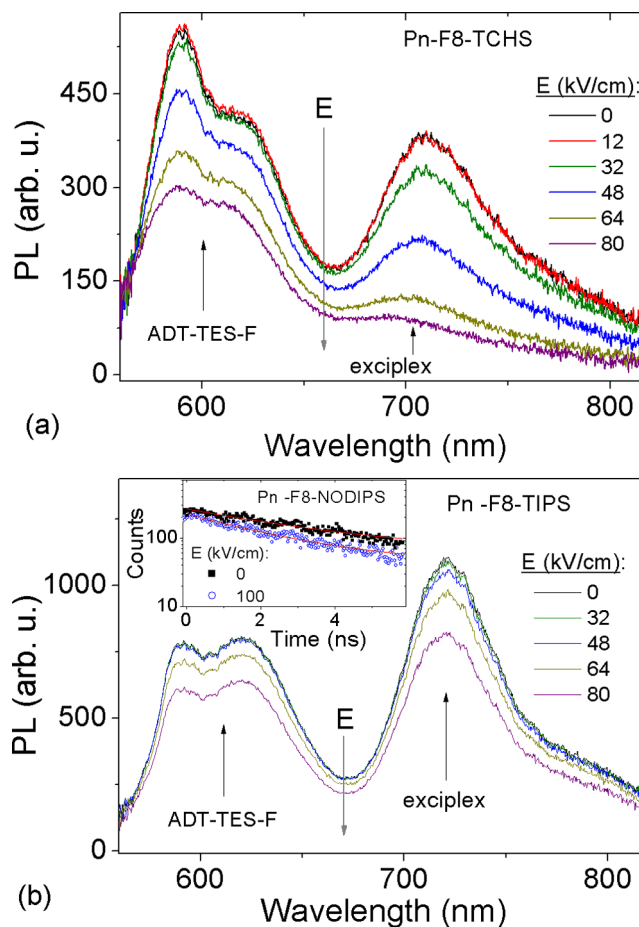


Figure 3. PL spectra of (a) an ADT-TES-F/Pn-F8-TCHS (2%) film and (b) an ADT-TES-F/Pn-F8-TIPS (2%) film at various applied electric fields. Spectral contributions corresponding to residual ADT-TES-F donor emission and to exciplex emission are indicated. Inset in panel b shows PL lifetime decays of the ADT-TES-F/Pn-F8-NODIPS exciplex in the absence of applied electric field and at 100 kV/cm. Single exponential fits ($I_{\text{PL}} \approx C \exp(-t/\tau)$) are also included. The fit parameters: $C = 206 \pm 3$ and $\tau = 3.43 \pm 0.08 \text{ ns}$ in the absence of the electric field and $C = 183 \pm 2$ and $\tau = 2.52 \pm 0.05 \text{ ns}$ at 100 kV/cm, which indicates both electric-field-assisted exciplex dissociation (change in τ) and dissociation of a precursor state to the exciplex (change in C).

The exciplex exhibited peak PL emission at an energy E_{CT} closely matching the energy gap between the LUMO of the A and the HOMO of the D, E_{DA} (Table 1) and a longer PL lifetime (e.g., $\sim 3.2\text{--}3.4 \text{ ns}$, $4.3\text{--}4.6 \text{ ns}$, and $\sim 19\text{--}22 \text{ ns}$ in composites with Pn-F8-NODIPS, Pn-F8-TIPS, and ADT-TIPS-CN acceptors, respectively) than that of ADT-TES-F excitons in pristine D films ($\sim 1.3 \text{ ns}$).³⁴ The energy of CT states E_{CT} in D/A composites has been discussed in the literature in the case of polymer-based blends.²⁷ In these materials, E_{CT} was found to be $\sim 0.3 \text{ eV}$ higher than E_{DA} , which was corrected for the difference between the HOMO–LUMO gap (E_{gap}) obtained from CV and $E_{\text{opt,gap}}$ of the D and A obtained from optical measurements.²⁷ In our small-molecule BHJs, the E_{CT} was considerably closer to the E_{DA} (Table 2), which, similar to observations in Section 3.1, suggests a

considerably smaller change in Coulomb interaction energy from an intra- to intermolecular exciton.

The strongest exciplex emission was observed in the composite with ADT-TIPS-CN (small D/A separation and the lowest ΔLUMO of all composites), in which most of the emission originated from the exciplex, whereas that of the D was almost completely quenched (Figure S5(a) of the Supporting Information).^{34,35} Exciplex emission and quenching of D emission were considerably weaker in the composites with Pn-F8-R than those with ADT-TIPS-CN (Table 1 and Figure 3). In addition, a factor of ~ 10 (~ 3.3) stronger exciplex emission was observed in the composite with Pn-F8-TIPS as compared with that with Pn-F8-TCHS (Pn-F8-NODIPS). This trend strongly correlates with the size of the acceptor's side group R, such that a larger D/A separation at the D/A interface corresponds to a less emissive exciplex.²⁴

In all composite films with A such that $\Delta\text{LUMO} > 0.6$ eV (0.65–0.95 eV, Table 2), there was no evidence of exciplex emission. Additionally, no signature of energy transfer from D to A characterized by emission from the acceptor was observed, and only the residual PL from the ADT-TES-F donor was present (e.g., Figures S6 and S7 of the Supporting Information) in these composites. In previously studied ADT-TES-F/ C_{60} (2%) D/A films ($\Delta\text{LUMO} = 1.45$ eV), a factor of 5–10 reduction in the PL (depending on the film preparation method) was observed, as compared with that in pristine D films, and attributed to fast photoinduced charge transfer from the D to A into charge-separated states, which resulted in a factor of ~ 3 improvement in fast charge carrier photogeneration.^{35,50} A considerably weaker PL quenching of the D, up to a factor of ~ 1.6 , was observed in the composites under study with PCBM, Hex-F8-TCHS, and IF-R acceptors. Assuming that the PL quenching of the D is due to charge transfer from D to A, this suggests that charge transfer in these composites is considerably less efficient than in those with C_{60} , which could be due to smaller ΔLUMOs .

To explore the propensity of emissive states to dissociate under applied electric fields (E fields), we measured PL spectra at various E fields and obtained the PL quenching parameter $Q(E) = 1 - I_{\text{PL}}(E)/I_{\text{PL}}(0)$, where $I_{\text{PL}}(E)$ and $I_{\text{PL}}(0)$ are integrated PL spectra at the field value E and in the absence of applied electric field, respectively. Spectra were integrated in the PL spectral ranges of the D and, when applicable, of the exciplex. Considerably higher E -field-assisted quenching Q , of both D exciton and exciplex emission (filled and open symbols in Figure 4, respectively), was observed in composites with larger D/A separations, such as those with PCBM or derivatives that have TCHS side groups, as compared with those with derivatives with TIPS side groups or pristine D films (Figures 3, Figures S4(a) and S5(a) of the Supporting Information).⁵¹ A reduction in the PL lifetimes, of both the exciplex and D exciton, upon an increase in E field, was observed in all samples. For example, the PL lifetimes of the exciplex in composites with Pn-F8-NODIPS (Pn-F8-TIPS) decreased from 3.4 ns (4.6 ns) in the absence of E field to 2.5 ns (3.8 ns) at 100 kV/cm (inset of Figure 3b). Under similar conditions, the PL lifetimes of the D exciton in composites with PCBM (pristine D films) decreased from 1.8 (1.3 ns) to 1.2 ns (1.1 ns). This confirmed that most of the PL quenching Q in Figure 4 is due to the exciplex and D exciton dissociation. In the case of the exciplex, the increase in Q with a D/A separation is consistent with a smaller exciplex binding energy resulting from the larger D/A separation and thus more efficient dissociation under E fields.¹⁷

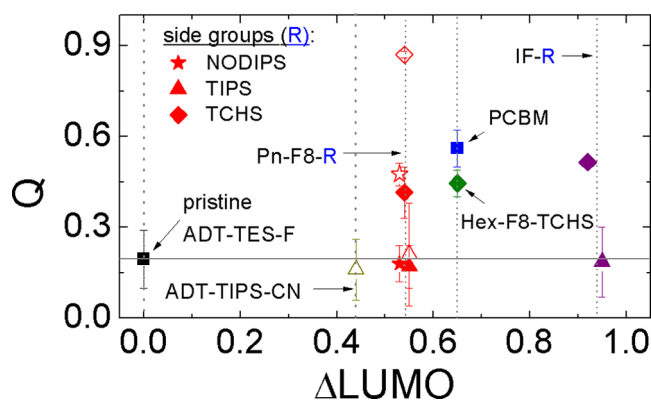


Figure 4. Electric-field-assisted PL quenching Q at 100 kV/cm in pristine ADT-TES-F (pristine D) films ($\Delta\text{LUMO} = 0$) and in composites. Filled and open symbols correspond to the D exciton and exciplex emission, respectively. Error bars reflect sample-to-sample variation. Considerably higher values of Q are observed in composites with larger D/A separation.

The similar trend observed in Q for the D exciton indicates that in composites with large D/A separation, excitons on D molecules near the D/A interface contribute significantly to the PL and are considerably more prone to dissociation, as compared with D excitons in pristine D films or in composites with acceptors that have TIPS side groups. A reduction in the amplitude of the PL lifetime decays was also observed for both the exciplex and D exciton. In both cases, it was more pronounced in composites with a larger D/A separation; for example, an amplitude reduction of $\sim 11\%$ ($< 1\%$) in composites with the Pn-F8-NODIPS (Pn-F8-TIPS) exciplex and of $\sim 20\%$ (8%) in the D exciton in the composite with PCBM (pristine D films) was observed. This suggests that the efficiency of E -field-assisted dissociation of a precursor state to both the exciplex and D exciton is also affected by the D/A separation.

3.3. Transient Photocurrent. To understand the relationship between the exciton dissociation (both exciplex and D exciton) observed in PL and charge-carrier photogeneration, we measured photocurrents in films under pulsed (355 nm, 500 ps) photoexcitation as a function of applied E field (Section 2.4). In pristine D films, at all values of applied E field, transient photocurrents (I_{ph}) with a sub-0.6 ns rise time, limited by the time resolution of the setup, were obtained (Table 2 and Figure S4(b) of the Supporting Information). This indicates fast (most likely sub-30 ps or below)^{52–55} charge-carrier photogeneration, consistent with previous studies of similar films.^{35,38,53} Because charge photogeneration occurred faster than D exciton dissociation, assessed in measurements of PL lifetime decays, at all E fields, most of the photogenerated carriers contributing to the peak of I_{ph} originated from the dissociation of a state, which is a precursor to the emissive D exciton.³⁵ After peak photogeneration, the I_{ph} transient exhibited a fast initial decay, due to carrier trapping and recombination, followed by a slow power-law decay that persisted up to at least ~ 2 μs , as in previous studies.^{50,53} In all films, the fast decay component was electric-field-dependent, which is most likely due to field-dependent charge carrier mobility³⁵ that results in field-dependent charge carrier trapping and recombination rates. In composites with small D/A separation (acceptors with TIPS side groups), a sub-0.6 ns rise time of the I_{ph} was observed at all E fields (Table 2 and Figures 5a and 6a), similar to pristine D films. Thus, most of the photogenerated carriers contributing to

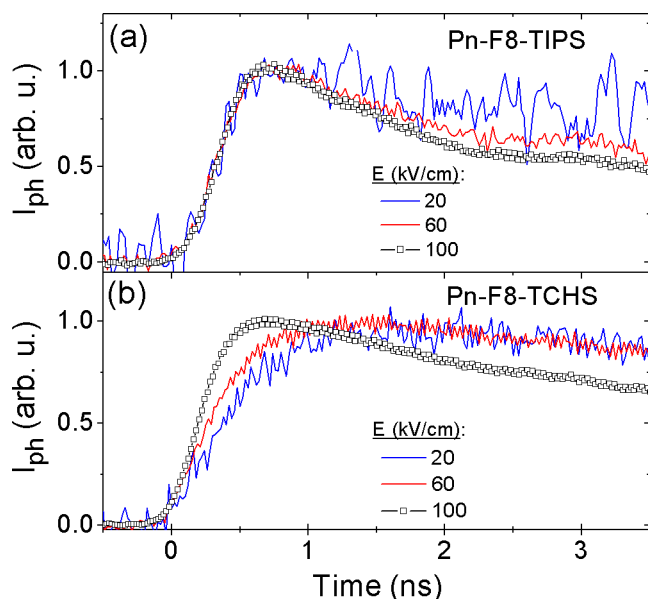


Figure 5. Transient photocurrents (I_{ph}) measured under 355 nm, 500 ps pulsed excitation, normalized by their peak values at several applied electric fields in composites with (a) Pn-F8-TIPS and (b) Pn-F8-TCHS acceptors.

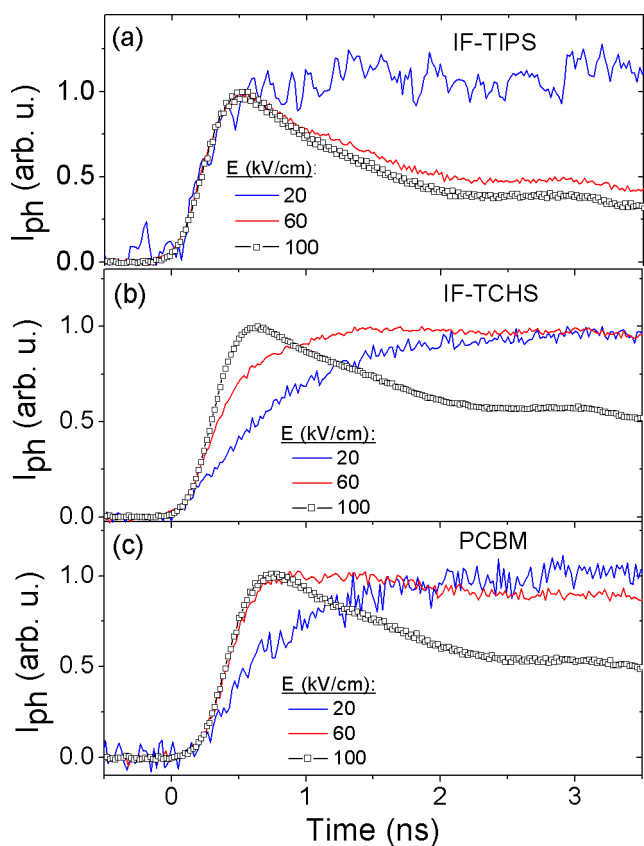


Figure 6. Transient photocurrents (I_{ph}) measured under 355 nm, 500 ps pulsed excitation, normalized by their peak values at several applied electric fields in composites with (a) IF-TIPS, (b) IF-TCHS, and (c) PCBM acceptors.

the peak of I_{ph} were produced by dissociation of a state that is a precursor to the D exciton, as in pristine D films, and the contribution of exciplex dissociation to I_{ph} was small. In

contrast, in composites with a larger D/A separation, the rise time of I_{ph} was highly E -field-dependent (Figures 5b and 6b,c and Table 2). For example, in composites with Pn-F8-TCHS or Pn-F8-NODIPS acceptors (Figure 5b), the peak of I_{ph} at 20 kV/cm occurred at times $t_{ph,max} \approx 2.4$ and 3.3 ns, respectively, consistent with the time scales of exciplex lifetimes in Pn-F8-R composites (e.g., inset of Figure 3b), whereas the charge photogeneration was considerably faster (<0.6 ns) at 100 kV/cm. Interestingly, at 20 kV/cm, a similarly slow photocurrent rise (with $t_{ph,max} \approx 2.2$ to 3.3 ns) was observed in composites that did not exhibit any exciplex emission (i.e., those with Hex-F8-TCHS, PCBM, and IF-TCHS acceptors (Table 2 and Figure 6b,c)). A possible explanation for this behavior is the existence of a nonemissive CT state with a lifetime of several nanoseconds at the D/A interface in these composites, similar to that reported in a variety of polymer-based blends.²⁷

Regardless of the emission properties of the CT exciton in our composites, the following picture of nanosecond time-scale charge photogeneration emerged. The photoexcitation of the D results in the formation of a precursor state to the D exciton, followed by the competition between sub-0.6 ns charge-carrier photogeneration and CT exciton formation.^{56,57} At low E fields (≤ 60 kV/cm), a range that is relevant for photovoltaics,⁶ the CT exciton formation prevails and is followed by slow charge carrier generation via E -field-assisted dissociation. Because the CT exciton dissociation is more efficient in composites with a larger D/A separation,¹⁷ a small improvement in charge photogeneration (of up to factor of 2 at 40 kV/cm at $\Delta LUMO = 0.92$ eV, depending on the $\Delta LUMO$, filled symbols in Figure 7) is observed in these composites as compared with

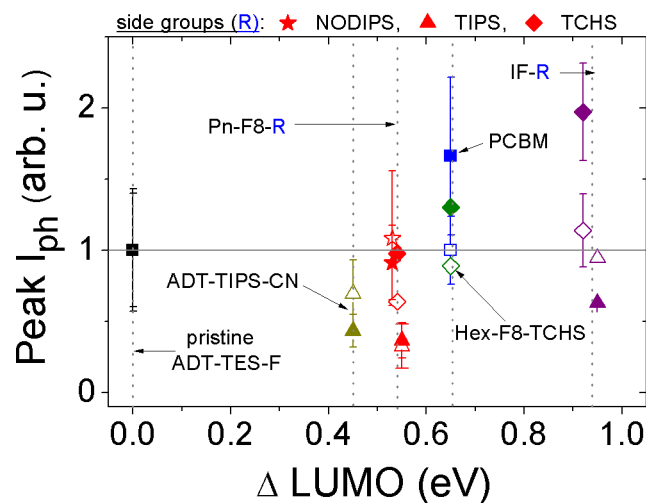


Figure 7. Peak transient photocurrents (I_{ph}) obtained in composites at 40 (filled symbols) and 100 kV/cm (open symbols) under 355 nm, 500 ps excitation, normalized by corresponding values measured in pristine ADT-TES-F (pristine D) films. Error bars correspond to sample-to-sample variation.

pristine D films. This trend is consistent with previous observations of a factor of 3 increase in the peak of I_{ph} in ADT-TES-F/ C_{60} (2%) composites ($\Delta LUMO = 1.45$ eV) as compared with pristine D films.⁵⁰ In contrast, the CT exciton dissociation is not efficient in composites with acceptors having TIPS side groups, and thus a reduction in charge photogeneration efficiency is observed in these composites, as compared with pristine D films (Figure 7, filled symbols, 40 kV/cm). At high E fields (>60 kV/cm), a range that is relevant,

for example, for photorefractive applications,⁵ fast carrier photogeneration from the precursor state to the pristine D and CT excitons dominates over the CT exciton formation in all composites, and no increase in charge photogeneration efficiency in composites as compared with pristine D films is observed (open symbols in Figure 7, 100 kV/cm).

Figure 8a shows the effect of the A on charge-carrier recombination. In all composites with a larger D/A separation

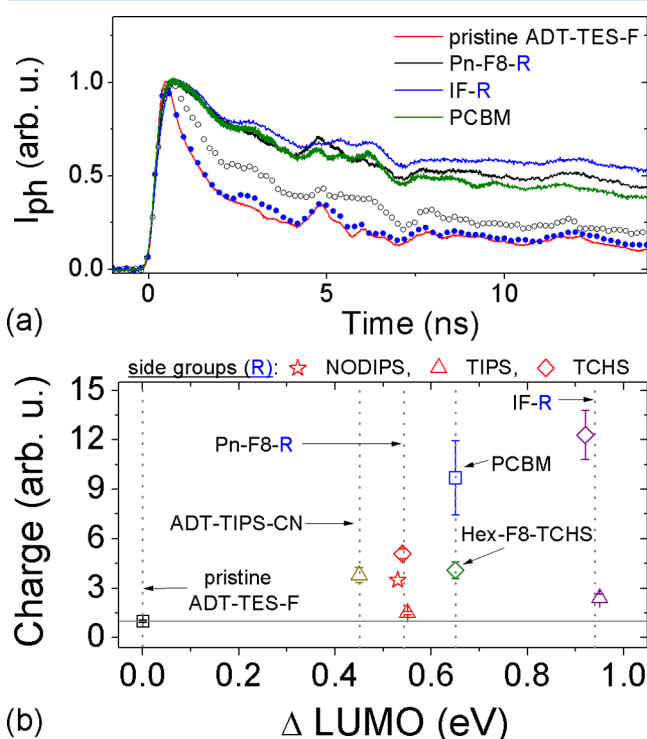


Figure 8. (a) Normalized transient photocurrents measured at 100 kV/cm in a pristine ADT-TES-F (pristine D) film (red line) and in composites with Pn-F8-R (black line and open squares for R = TCHS and TIPS, respectively), IF-R (blue line and filled circles for R = TCHS and TIPS, respectively), and PCBM (green line). (b) Total mobile charge in composites obtained by integrating transient photocurrents, measured under 355 nm, 500 ps pulsed excitation at 80 kV/cm, over $\sim 2 \mu$ s, normalized by corresponding values in pristine ADT-TES-F (pristine D) films. Error bars correspond to sample-to-sample variation.

(i.e., with PCBM or derivatives with TCHS or NODIPS side groups), at the same electric field, the initial decay of the transient photocurrent was considerably slower than that in pristine D films or in composites with A that have TIPS side groups, indicative of inhibited charge-carrier recombination. For example, at 100 kV/cm, only $\sim 11\%$ of initially generated charge carriers remained mobile at ~ 10 ns after photoexcitation in the pristine D films; this number increased to $\sim 45\%$ in composites with Pn-F8-TCHS and PCBM acceptors and to 53% in those with IF-TCHS. Figure 8b shows the amount of mobile charge obtained by integrating photocurrent transients measured at 80 kV/cm over the time scale of $\sim 2 \mu$ s in composites, normalized by those in pristine D films. In all composites, the inhibited recombination led to a higher total charge as compared with that in pristine D films, with the highest increase (by a factor of ~ 4 –12) in composites with a larger D/A separation (i.e., with PCBM and derivatives with TCHS side groups).

3.4. cw Photocurrent. Figure 9 shows cw photocurrents (I_{cw}) obtained at 532 nm and a broad-band 300–400 nm

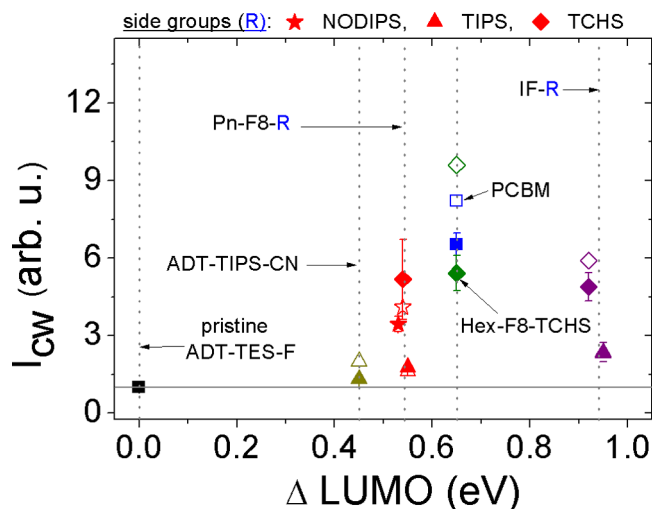


Figure 9. Photocurrents obtained under 532 and 300–400 nm (peaked at ~ 370 nm) cw photoexcitation (filled and open symbols, respectively) at 40 kV/cm, normalized by corresponding values measured in pristine ADT-TES-F (pristine D) films. Error bars correspond to sample-to-sample variation.

(peaked at ~ 370 nm) excitation (filled and open symbols, respectively) at an E field of 40 kV/cm in composites, normalized by those in pristine D films. An increase in I_{cw} was observed in all composites as compared with pristine D films, with a larger increase (by a factor of 5–10) achieved in composites with a larger D/A separation (i.e., those with PCBM or derivatives with TCHS side groups), as compared with that of a factor of 1.8 to 2.5 in composites with smaller D/A separation (i.e., those with derivatives that have TIPS side groups). In keeping with the insights obtained from time-resolved photocurrents in Figures 7 and 8b, we attribute most of the increase in I_{cw} in composites to inhibited charge recombination rather than to improved photogeneration efficiency. The overall trends in I_{cw} at both 532 and ~ 370 nm excitation, can be summarized as follows: (i) no particular dependence of I_{cw} on the Δ LUMO in composites with large D/A separation and a slight increase in I_{cw} with Δ LUMO (by a factor of ~ 1.5 from a Δ LUMO of 0.44 to 0.95 eV) in composites with small D/A separation and (ii) considerably stronger dependence of the I_{cw} on the D/A separation as compared with effects of the Δ LUMO. This suggests that it should be possible to optimize the CT properties of BHJs by controlling the molecular arrangement at the interface^{17,18} without a need to further increase the D/A LUMO offset, which is often detrimental to the open circuit voltage in solar cells.⁶

4. SUMMARY

In summary, composite films of small molecules with Δ LUMO of <0.6 and >0.6 eV exhibited exciplex and nonemissive CT state formation, respectively. E -field-assisted PL quenching of the exciplex and of the D exciton dramatically depended on the D/A separation. A competition between sub-0.6 ns charge-carrier photogeneration and CT exciton formation was observed, with outcomes depending on the applied E field and on the spatial D/A separation. At low E fields, CT

formation was dominant, and up to a factor of 2 increase in charge photogeneration efficiency due to CT exciton dissociation was observed in composites with large spatial D/A separation, as compared with that in pristine D films. At high E fields, the fast charge-carrier photogeneration was dominant in all composites, and no improvement in charge photogeneration efficiency with respect to that in pristine D films was observed. Dramatic changes in charge carrier recombination dynamics were observed depending on the spatial D/A separation. These contributed to up to a factor of 5–10 improvement in cw photocurrents in composites with large D/A separation, as compared with those in pristine D films. Our studies show that it is possible to control properties of CT states and their contribution to the photocurrent by optimizing morphology of the D/A interface. In particular, both CT dissociation and charge carrier recombination can be effectively manipulated by adjusting the molecular interaction between the D and A by changing the size of the substituent on the A, without needing to increase ΔLUMO (at least for $\Delta\text{LUMO} > 0.5$ eV) to improve the photocurrent; this could enable, for example, maximizing the open circuit voltage in solar cells. In applications that rely on applied E fields, it should be possible to manipulate contributions of CT excitons to the photocurrent by changing the E field and thus tune charge photogeneration dynamics and efficiency to satisfy particular requirements.

■ ASSOCIATED CONTENT

■ Supporting Information

Synthesis and characterization of IF-TCHS, X-ray diffraction data, optical absorption and PL spectra of molecules and selected composites, and PL spectra and transient photocurrents at various applied electric fields for pristine ADT-TES-F and several composites. The material is available free of charge via the Internet at <http://pubs.acs.org>.

■ AUTHOR INFORMATION

Corresponding Author

*E-mail: oksana@science.oregonstate.edu.

Notes

The authors declare no competing financial interest.

■ ACKNOWLEDGMENTS

We thank T. Sharf for photolithography of device substrates. This work was supported by NSF (CAREER) program (DMR-0748671) to O.O., NSF (CHE-1013032) to M.M.H., NSF (DMR-1035257) to J.E.A., and ONR grant N0014-07-1-0457.

■ ABBREVIATIONS

HOMO, highest occupied molecular orbital; LUMO, lowest unoccupied molecular orbital; D, donor; A, acceptor; BHJ, bulk heterojunction; PL, photoluminescence; CT, charge transfer; cw, continuous wave; ADT, anthradithiophene; Pn, pentacene; Hex, hexacene; IF, indeno[1,2-*b*]fluorene; PCBM, [6,6]-phenyl- C_{61} -butyric acid methyl ester; PMMA, poly(methylmethacrylate); ADT-TES-F, fluorinated ADT functionalized with (triethylsilyl)ethynyl side groups; ADT-TIPS-CN, ADT with cyano end groups and functionalized with (triisopropylsilyl)ethynyl side groups; TIPS, (triisopropylsilyl)ethynyl; NODIPS, (*n*-octyldiisopropylsilyl)ethynyl; TCHS, (tricyclohexylsilyl)ethynyl

■ REFERENCES

- (1) Forrest, S. R. *Nature* **2004**, *428*, 911.
- (2) Katz, H. E.; Huang, J. *Annu. Rev. Mater. Res.* **2009**, *39*, 71.
- (3) Heeger, A. J. *Chem. Soc. Rev.* **2010**, *39*, 2354.
- (4) Kim, Y.; Ballarotto, M.; Park, D.; Du, M.; Cao, W.; Lee, C. H.; Herman, W. N.; Romero, D. B. *Appl. Phys. Lett.* **2007**, *91*, 193510.
- (5) Ostroverkhova, O.; Moerner, W. E. *Chem. Rev.* **2004**, *104*, 3267.
- (6) Clarke, T. M.; Durrant, J. R. *Chem. Rev.* **2010**, *110*, 6736.
- (7) Walker, B.; Kim, C.; Nguyen, T. Q. *Chem. Mater.* **2011**, *23*, 470.
- (8) Anthony, J. E. *Chem. Mater.* **2011**, *23*, 583.
- (9) Roncali, J. *Acc. Chem. Res.* **2009**, *42*, 1719.
- (10) Lloyd, M. T.; Anthony, J. E.; Malliaras, G. G. *Mater. Today* **2007**, *10*, 34.
- (11) Sun, Y.; Welch, G.; Leong, W.; Takacs, C.; Bazan, G.; Heeger, A. J. *Nat. Mater.* **2012**, *11*, 44.
- (12) Mishra, A.; Bauerle, P. *Angew. Chem., Int. Ed.* **2012**, *51*, 2020.
- (13) Lim, Y. F.; Shu, Y.; Parkin, S. R.; Anthony, J. E.; Malliaras, G. G. *J. Mater. Chem.* **2009**, *19*, 3049.
- (14) Shu, Y.; Lim, Y. F.; Li, Z.; Purushothaman, B.; Hallani, R.; Kim, J. E.; Parkin, S. R.; Malliaras, G. G.; Anthony, J. E. *Chem. Sci.* **2011**, *2*, 363.
- (15) Shoaee, S.; Eng, M. P.; Espildora, E.; Delgado, J. L.; Campo, B.; Martin, N.; Vanderzande, D.; Durrant, J. R. *Energy Environ. Sci.* **2010**, *3*, 971.
- (16) Ohkita, H.; Cook, S.; Astuti, Y.; Duffy, W.; Tierney, S.; Zhang, W.; Heeney, M.; McCulloch, L.; Nelson, J.; Bradley, D. D. C.; Durrant, J. R. *J. Am. Chem. Soc.* **2008**, *130*, 3030.
- (17) Holcombe, T. W.; Norton, J. E.; Rivnay, J.; Woo, C. H.; Goris, L.; Pilego, C.; Griffini, G.; Sellinger, A.; Bredas, J. L.; Salleo, A.; Frechet, J. M. J. *J. Am. Chem. Soc.* **2011**, *133*, 12106.
- (18) Beljonne, D.; Cornil, J.; Muccioli, L.; Zannoni, C.; Bredas, J. L.; Castet, F. *Chem. Mater.* **2011**, *23*, 591.
- (19) Beaujuge, P. M.; Frechet, J. M. J. *J. Am. Chem. Soc.* **2011**, *133*, 20009.
- (20) Deibel, C.; Strobel, T.; Dyakonov, V. *Adv. Mater.* **2010**, *22*, 4097.
- (21) Bredas, J. L.; Norton, J. E.; Cornil, J.; Coropceanu, V. *Acc. Chem. Res.* **2009**, *42*, 1691.
- (22) Zhu, X. Y.; Yang, Q.; Muntwiler, M. *Acc. Chem. Res.* **2009**, *42*, 1779.
- (23) Paquin, F.; Latini, G.; Sakowicz, M.; Karsenti, P. L.; Wang, L.; Beljonne, D.; Stingelin, N.; Silva, C. *Phys. Rev. Lett.* **2011**, *106*, 197401.
- (24) Morteaux, A. C.; Sreearunothai, P.; Herz, L. M.; Friend, R. H.; Silva, C. *Phys. Rev. Lett.* **2004**, *92*, 247402.
- (25) Veldman, D.; Ipek, O.; Meskers, S. C. J.; Sweelssen, J.; Koetse, M. M.; Veenstra, S. C.; Kroon, J. M.; van Bavel, S. S.; Loos, J.; Janssen, R. A. J. *J. Am. Chem. Soc.* **2008**, *130*, 7721.
- (26) Lee, J.; Vandewal, K.; Yost, S. R.; Bahlke, M. E.; Goris, L.; Baldo, M. A.; Manca, J.; Van Voorhis, T. *J. Am. Chem. Soc.* **2010**, *132*, 11878.
- (27) Veldman, D.; Meskers, S. C. J.; Janssen, R. A. J. *Adv. Funct. Mater.* **2009**, *19*, 1939.
- (28) Pensack, R. D.; Asbury, J. B. *Chem. Phys. Lett.* **2011**, *515*, 197.
- (29) Devizis, A.; Serbenta, A.; Peckus, D.; Thiessen, A.; Alle, R.; Meerholz, K.; Hertel, D.; Gulbinas, V. *J. Chem. Phys.* **2010**, *133*, 164904.
- (30) Yin, C.; Kietzke, T.; Neher, D.; Horhold, H. H. *Appl. Phys. Lett.* **2007**, *90*, 133502.
- (31) Bakulin, A. A.; Rao, A.; Pavelyev, V. G.; van Loosdrecht, P. H. M.; Pshenichnikov, M. S.; Niedzialek, D.; Cornil, J.; Beljonne, D.; Friend, R. H. *Science* **2012**, *335*, 1340.
- (32) Faist, M. A.; Kirchartz, T.; Gong, W.; Ashraf, R. S.; McCulloch, I.; de Mello, J. C.; Ekins-Daukes, N. J.; Bradley, D. D. C.; Nelson, J. J. *Am. Chem. Soc.* **2012**, *134*, 685.
- (33) Sanchez-Diaz, A.; Pacios, R.; Muncas, U.; Torres, T.; Palomares, E. *Org. Electron.* **2011**, *12*, 329.
- (34) Shepherd, W. E. B.; Platt, A. D.; Kendrick, M. J.; Loth, M. A.; Anthony, J. E.; Ostroverkhova, O. *J. Phys. Chem. Lett.* **2011**, *2*, 362.
- (35) Platt, A. D.; Kendrick, M. J.; Loth, M.; Anthony, J. E.; Ostroverkhova, O. *Phys. Rev. B* **2011**, *84*, 235209.

- (36) Park, S. K.; Mourey, D. A.; Subramanian, S.; Anthony, J. E.; Jackson, T. N. *Appl. Phys. Lett.* **2008**, *93*, 043301.
- (37) Gundlach, D. J.; Royer, J. E.; Park, S. K.; Subramanian, S.; Jurchescu, O. D.; Hamadani, B. H.; Moad, A. J.; Kline, R. J.; Teague, L. C.; Kirillov, O.; Richter, C. A.; Kushmerick, J. G.; Richter, L. J.; Parkin, S. R.; Jackson, T. N.; Anthony, J. E. *Nat. Mater.* **2008**, *7*, 216.
- (38) Platt, A. D.; Day, J.; Subramanian, S.; Anthony, J. E.; Ostroverkhova, O. *J. Phys. Chem. C* **2009**, *113*, 14006.
- (39) Shepherd, W. E. B.; Platt, A. D.; Hofer, D.; Ostroverkhova, O.; Loth, M.; Anthony, J. E. *Appl. Phys. Lett.* **2010**, *97*, 163303.
- (40) Anthony, J. E.; Eaton, D. L.; Parkin, S. R. *Org. Lett.* **2002**, *4*, 15.
- (41) Anthony, J. E.; Brooks, J. S.; Eaton, D. L.; Parkin, S. R. *J. Am. Chem. Soc.* **2001**, *123*, 9482.
- (42) Swartz, C. R.; Parkin, S. R.; Bullock, J. E.; Anthony, J. E.; Mayer, A. C.; Malliaras, G. G. *Org. Lett.* **2005**, *7*, 3163.
- (43) Purushothaman, B.; Park, S. R.; Kendrick, M. J.; David, D.; Ward, J. W.; Yu, L.; Stingelin, N.; Jurchescu, O. D.; Ostroverkhova, O.; Anthony, J. E. *Chem. Commun.* **2012**, *48*, 8261.
- (44) Chase, D. T.; Fix, A. G.; Rose, B. D.; Weber, C. D.; Nobusue, S.; Stockwell, C. E.; Zakharov, L. N.; Lonergan, M. C.; Haley, M. M. *Angew. Chem., Int. Ed.* **2011**, *50*, 11103.
- (45) Chase, D. T.; Rose, B. D.; McClintock, S. P.; Zakharov, L. N.; Haley, M. M. *Angew. Chem., Int. Ed.* **2011**, *50*, 1127.
- (46) Kline, R. J.; Hudson, S. D.; Zhang, X. R.; Gundlach, D. J.; Moad, A. J.; Jurchescu, O. D.; Jackson, T. N.; Subramanian, S.; Anthony, J. E.; Toney, M. F.; Richter, L. J. *Chem. Mater.* **2011**, *23*, 1194.
- (47) Kleemann, H.; Schuenemann, C.; Zakhidov, A. A.; Riede, M.; Lussem, B.; Leo, K. *Org. Electron.* **2012**, *13*, 58.
- (48) Veldman, D.; Bastiaansen, J.; Lageveld-Voss, B.; Sweelssen, J.; Koetse, M.; Meskers, S. C. J.; Janssen, R. A. J. *Thin Solid Films* **2006**, *511–512*, 581.
- (49) Halls, J. J. M.; Cornil, J.; dos Santos, D. A.; Silbey, R. J.; Hwang, D. H.; Holmes, A. B.; Bredas, J. L.; Friend, R. H. *Phys. Rev. B* **1999**, *60*, 5721.
- (50) Day, J.; Platt, A. D.; Ostroverkhova, O.; Subramanian, S.; Anthony, J. E. *Appl. Phys. Lett.* **2009**, *94*, 013306.
- (51) Rispens, M. T.; Meetsma, A.; Rittberger, R.; Brabec, C. J.; Sariciftci, N. S.; Hummelen, J. C. *Chem. Commun.* **2003**, 2116.
- (52) Day, J.; Subramanian, S.; Anthony, J. E.; Lu, Z.; Twieg, R. J.; Ostroverkhova, O. *J. Appl. Phys.* **2008**, *103*, 123715.
- (53) Day, J.; Platt, A. D.; Subramanian, S.; Anthony, J. E.; Ostroverkhova, O. *J. Appl. Phys.* **2009**, *105*, 103703.
- (54) Cooke, D. G.; Krebs, F. C.; Jepsen, P. U. *Phys. Rev. Lett.* **2012**, *108*, 056603.
- (55) Ostroverkhova, O.; Cooke, D. G.; Shcherbyna, S.; Egerton, R. F.; Hegmann, F. A.; Tykwinski, R. R.; Anthony, J. E. *Phys. Rev. B* **2005**, *71*, 035204.
- (56) Tsutsumi, J.; Yamada, T.; Matsui, H.; Haas, S.; Hasegawa, T. *Phys. Rev. Lett.* **2010**, *105*, 226601.
- (57) Etzold, F.; Howard, I. A.; Mauer, R.; Meister, M.; Kim, T. D.; Lee, K. S.; Baek, N. S.; Laquai, F. *J. Am. Chem. Soc.* **2011**, *133*, 9469.